J. Fluid Mech. (1993), *vol.* 256, *pp.* 403–426
Copyright © 1993 Cambridge University Press

Fundamental–subharmonic interaction: effect of phase relation

By M. R. HAJJ[1], R. W. MIKSAD[2] AND E. J. POWERS[2]

[1] Department of Engineering Science and Mechanics, Virginia Polytechnic Institute and State University, Blacksburg, VA 24061-0219, USA

[2] College of Engineering, The University of Texas at Austin, Austin, TX 78712, USA

(Received 23 December 1991 and in revised form 21 April 1993)

The effect of the phase relation (i.e. phase difference and coupling) between the fundamental and subharmonic modes on the transition to turbulence of a mixing layer is investigated. Experiments are conducted to study the development of the subharmonic and fundamental modes under different phase-controlled excitations. Higher-order spectral moments are used to measure phase differences, levels of phase coupling, and energy transfer rates between the two modes at different downstream locations. Local measurements of the wavenumber–frequency spectra are used to examine the phase-speed matching conditions required for efficient energy transfer. The results show that when the phase coupling between the fundamental and the subharmonic is high, maximum subharmonic growth is found to occur at a critical phase difference close to zero. The subharmonic growth is found to result from a resonant parametric interaction between the fundamental and the subharmonic in which phase-speed matching conditions are satisfied. In contrast, when the phase coupling level is low, the phase difference is irregular and varying, the efficiency of parametric interactions is low, phase-speed matching conditions are not met and subharmonic growth is suppressed.

1. Introduction

Interactions between the fundamental and subharmonic instability modes which lead to subharmonic growth play an important role in the transition to turbulence of mixing layers. Ho & Huang (1982) showed that the subharmonic amplification region coincides with the region between vortex roll-up and vortex merging. In a naturally growing mixing layer, Hajj, Miksad & Powers (1992) showed that energy transfer to the subharmonic via the parametric interaction, where the energy is passed from the mean flow to the subharmonic as a result of parametric variations of the fundamental, dominates the quadratic mechanism, where the energy is passed directly from the fundamental. The analytical studies of Kelly (1967), Monkewitz (1988), Nikitopoulos & Liu (1987) and Mankbadi (1985) showed that subharmonic growth is a result of its interaction with the fundamental component and this interaction process is dependent on the amplitude of the fundamental mode and on the phase difference between the two modes. The problem of the effect of fundamental–subharmonic phase difference on the subharmonic growth has also been investigated numerically. Patnaik, Sherman & Corcos (1976) and Riley & Metcalfe (1980) showed that changing the phase difference between the fundamental and subharmonic modes leads to a shift from vortex merging to vortex shredding where the cores of the fundamental are destroyed by the straining field of the subharmonic.

Many experimental investigations have studied the characteristics of the subharmonic growth and the fundamental–subharmonic interaction mechanisms. In single-frequency excitation experiments, Freymuth (1966) and Ho & Huang (1982) showed that by varying the forcing frequencies and their levels, the locations of the saturation of the fundamental and its subharmonic can be controlled. Miksad (1972, 1973) observed that the saturation levels of the subharmonic and its fundamental vary under single- and double-frequency excitations. Zhang, Ho & Monkewitz (1983) showed that the subharmonic development and its saturation level are dependent on the phase difference between the fundamental and the subharmonic, and Arby & Ffowcs Williams (1984) showed that the subharmonic component can be either amplified or depressed depending on its phase difference with the fundamental. Hajj, Miksad & Powers (1991) demonstrated that as the phase difference between the fundamental and subharmonic modes is changed, the coupling between the fundamental and its subharmonic is altered and the growth of the subharmonic mode is affected. Yang & Karlsson (1991) showed that simultaneous excitation of the fundamental and the subharmonic may lead to vortex merging of different kinds (pairing or tearing) depending on the phase difference between the two modes. More recently, Rajaee & Karlsson (1992) used downstream measurements of the relative phases with respect to the driving signal, and amplitudes of the subharmonic, fundamental and their harmonics to show that the velocity field is dependent on the phase difference between the fundamental and subharmonic modes. Rajaee & Karlsson also measured the energy transfer rates between the different modes and the mean flow and showed that energy transfer to the subharmonic is affected by the phase difference between the fundamental and subharmonic modes and that energy transfer from the mean flow dominates that from the fundamental.

The importance of fundamental–subharmonic phase difference to the subharmonic development is clear and the thrust of this paper is to quantitatively establish whether a critical phase difference exists under which energy transfer to the subharmonic is most efficient. Since the flow and the structure of the interacting modes, including the relative phases, evolve with downstream distance, the work presented here focuses on local measurements of the phase difference and corresponding levels of fundamental–subharmonic phase couplings and energy transfer rates. This allows us to watch the evolving dynamics of interaction mechanisms and subharmonic development and identify the critical stages. In this investigation, a series of experiments with double-frequency excitations at the fundamental and subharmonic frequencies with different relative phases were conducted in order to quantify the effect of the fundamental–subharmonic phase relation, i.e. the phase difference and interaction coupling level, on the mechanisms responsible for subharmonic growth. Polyspectral analysis is used to quantify interaction coupling levels, phase differences and the corresponding linear, parametric and quadratic energy transfer rates. The results show that a critical phase difference exists for which energy transfer to the subharmonic is most efficient.

2. Experimental set-up and data analysis

The experiments were conducted in an open return, low-turbulence wind tunnel. The tunnel is driven from the downstream end by a positive displacement pump. The test section is isolated from the pump noise by a sonic throat and two resonating filters. A more detailed description of the characteristics of the contraction section, stilling chamber, and splitter plate is given in Hajj (1990) and a schematic of the facility is given in Hajj *et al.* (1992). The test section of the wind tunnel has a width of 30 cm, a height

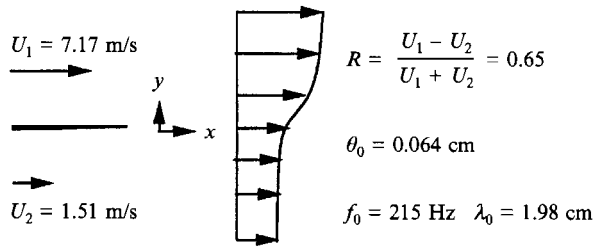

FIGURE 1. Schematic illustration of the free shear layer experimental conditions.

of 20 cm, and a length of 140 cm. The bottom wall of the test section is adjustable for downstream pressure gradient control. By adjusting this wall, downstream deviations of the upper and lower free-stream velocities were limited to less than 0.2% and 0.8% of their respective mean values. Limited spanwise measurements showed that velocity deviations in the spanwise direction were less than $\pm 0.45\%$ of the average velocity of the two streams. The high-speed stream was at 7.17 m/s and the low speed stream was at 1.51 m/s, see figure 1. This resulted in a velocity differential $\Delta U = U_1 - U_2 = 5.66$ m/s, and a velocity ratio, defined as $R = (U_1 - U_2)/(U_1 + U_2)$, equal to 0.65. The initial momentum thickness of the high-speed-side free-stream velocity, θ_0, was equal to 0.064 cm. Based on momentum thickness and the high-speed free-stream velocity, the Reynolds number was 305. At $x = 25.0$ cm, the width of the test section was $12.5\delta_w$ and at $x = 40.0$ cm, the width of the test section was $8.5\delta_w$, where δ_w is the local vorticity thickness. The measured frequency of the fundamental instability, f_0, was 215 Hz. The corresponding measured wavelength, λ_0, was 1.98 cm. The results presented here are for velocity fluctuations measured at the cross-stream locations of maximum u'_{rms} with a Disa 56C/N hot-wire anemometry system. A special probe (Jones *et al.* 1988) with two spatially separated sensing elements was used to measure energy transfer rates and frequency–wavenumber spectra. The spectral properties of the fluctuation field at each spatial point were calculated digitally from eight independent records. Each record consisted of simultaneous data from the two sensors and contained 4096 points sampled at a rate of 1000 Hz. This yielded a Nyquist frequency of 500 Hz. Power spectra were calculated using fast Fourier transform techniques. Ensemble averages over 64 realizations of 256 points each were used. This yielded a resolution bandwidth of 3.90 Hz. Estimates of the bicoherence were made by ensemble averaging over 256 realizations of 128 points each. This yielded a resolution bandwidth of 7.81 Hz. The downstream distance x is normalized with R/λ_0 as suggested by Huang & Ho (1990).

The fundamental and subharmonic modes were excited acoustically. The excitation system included a function generator controlled by an IBM–PC, a stereo amplifier, and two speakers. This set-up enabled us to control the relative amplitudes and phases between the fundamental and the subharmonic. Four different cases of phase-controlled excitations were studied. In each case, the phase of the subharmonic was set at zero while the phase of the fundamental was varied in $\frac{1}{2}\pi$ increments to establish four basic phase-difference experimental conditions. Figure 2 shows the spectral energy distribution in the free stream under the four different excitation conditions. The measured amplitudes of the fundamental and subharmonic modes in the free stream at $Rx/\lambda_0 = 0.06$ were of the order of $0.00014U_1$.

The amplitudes of the fundamental components along maximum u'_{rms} in the four cases of excitation at $Rx/\lambda_0 = 0.06$ were of the order of $0.0018U_1$. The amplitudes of the subharmonic were of the order of $0.0034U_1$. These values are about five times

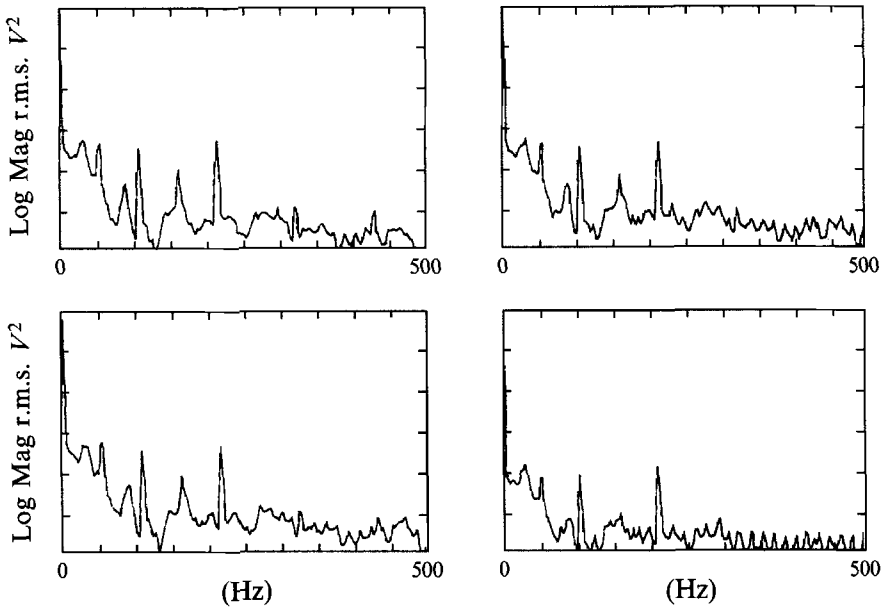

FIGURE 2. Spectral energy distribution under different excitation conditions at $Rx/\lambda_0 = 0.06$ in the free stream.

larger than the corresponding values under natural conditions. Corresponding values of the phase difference, based on the extrapolation of the values at $Rx/\lambda_0 = 0.3$ and 1.0 in the four cases are -0.27π, 0.24π, 0.69π, and 1.16π, respectively.

3. Effect of the phase relation

3.1. *Development and coupling of the spectral components – natural transition*

As shown in figures 3(*a*) and 3(*b*), the energy content at the fundamental and subharmonic frequencies vary in the cross-stream direction. These figures show the measured cross-stream variations of the energy of the fundamental and subharmonic modes at different downstream locations between $Rx/\lambda_0 = 0.06$ and 3.3. The dashed line in these figures traces the location of maximum u'_{rms} in the upper stream. Figure 3(*a*) shows that cross-stream variation of the energy of the fundamental mode is characterized by a double peak and a local minimum at the centreline. Figure 3(*b*) shows that the cross-stream variation of the energy of the subharmonic mode is characterized by a single peak at the centreline. The fundamental–subharmonic interaction is dependent on their respective amplitudes and relative phases. Because the amplitudes and phases of the fundamental and subharmonic modes vary in the cross-stream direction, it is expected that the coupling characteristics will also vary in the cross-stream direction. As shown by Hajj *et al.* (1992), the fundamental–subharmonic coupling characteristics can best be detected by the auto-bicoherence. A zero value of the auto-bicoherence indicates a low-coupling level between the two modes and a value near one indicates a high-coupling level. Figure 3(*c*) shows the cross-stream variations in the auto-bicoherence between the two modes. The results show that coupling variations in the cross-stream are characterized by a local peak at maximum u'_{rms}, which corresponds to a local maximum in the fundamental component distribution. The coupling variation is also characterized by a minimum at the centreline.

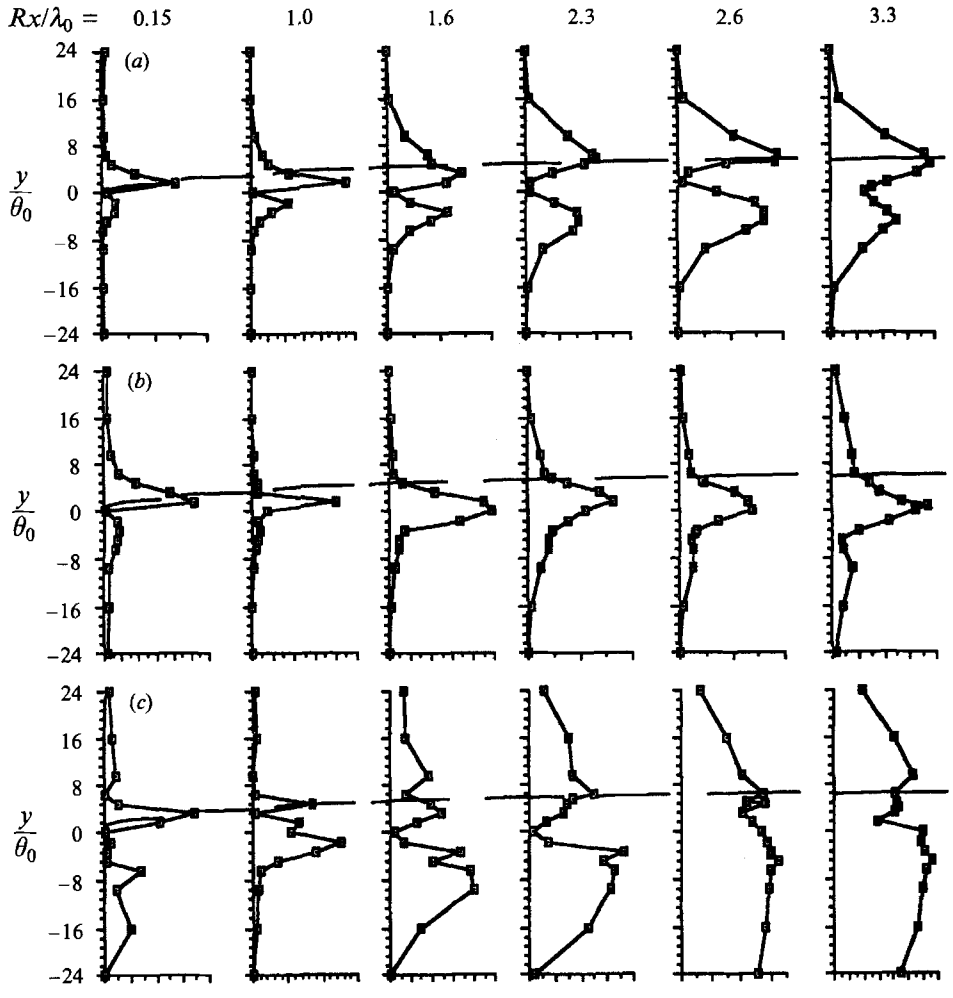

FIGURE 3. Cross-stream variations of (*a*) the energy of the fundamental mode, (*b*) the energy of the subharmonic mode and (*c*) the coupling level between the two modes under natural excitation conditions.

Ho *et al.* (1991) measured cross-stream variation in the level of phase jitter in the velocity signal. The results showed that fluctuations near the centreline are contaminated by small eddies and exhibit a high level of phase jitter when compared to cross-stream locations y/θ_0 between 4 and 10. This increase in the level of phase jitter with cross-stream variation from $y/\theta_0 = 4$ to the centreline in the results of Ho *et al.* (1991) is in qualitative agreement with the decrease in the coupling level between the fundamental and the subharmonic as the centreline is approached in our results. In the work presented here, the effects of the phase relation on fundamental–subharmonic interactions are measured at cross-stream locations corresponding to maxima in u'_{rms} and hence maximum fundamental–subharmonic coupling. It must be noted that, between $Rx/\lambda_0 = 1.3$ and 3.3, locations of maximum u'_{rms} correspond to a cross-stream location of y/θ_0 that varies between 3.5 and 8. This corresponds to the region defined by Ho *et al.* (1991) where phase jitter is minimum.

The development of the fundamental and subharmonic modes under 'natural' excitation conditions, along maximum u'_{rms}, is shown in figure 4. The characteristics of

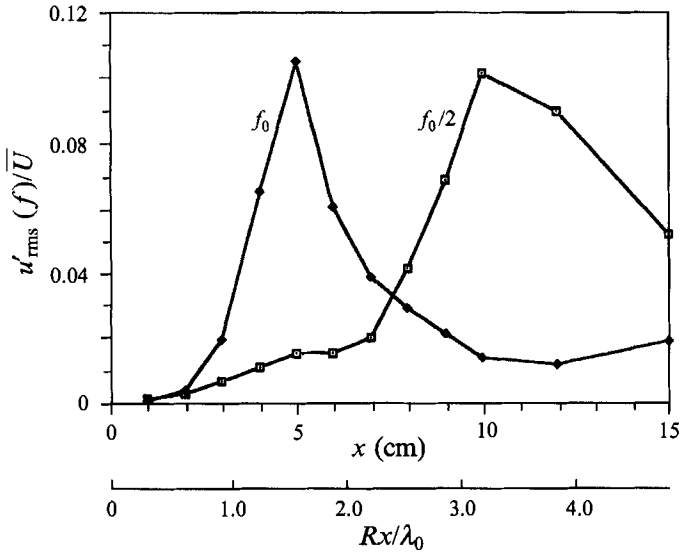

FIGURE 4. Downstream development of the fundamental and subharmonic modes under natural excitation conditions.

growing, saturating and decaying fundamental and subharmonic modes are similar to those observed in the experiments of Miksad (1972, 1973), Ho & Huang (1982), and many others. Initially, up to $Rx/\lambda_0 = 1.0$, both modes grow exponentially at rates close to those predicted by linear stability theory. At $Rx/\lambda_0 = 1.3$, the fundamental mode starts to equilibrate. Ho & Huang (1982) showed that the beginning of the saturation of the fundamental marks the vortex roll-up as observed in flow visualization experiments. While the fundamental is saturating, the subharmonic equilibrates, between $Rx/\lambda_0 = 1.3$ and 2.0. At this location, the amplitude of the subharmonic resumes its increase. The growth of the subharmonic continues until it reaches saturation at $Rx/\lambda_0 = 3.2$. The beginning of the saturation of the subharmonic has been related to the vortex merging process (Ho & Huang 1982).

The region between $Rx/\lambda_0 = 1.3$ and 3.2 is particularly important in the development and growth of the mixing layer. By $Rx/\lambda_0 = 1.3$, the fundamental mode has developed into a finite-amplitude wave that starts to roll up to form the first coherent structure observed in the mixing layer. Between $Rx/\lambda_0 = 1.3$ and 3.2, the local momentum thickness of the mixing layer doubles and the energy extraction from the mean flow increases significantly (Hajj *et al.* 1992). Previous experimental results suggest that in this region, the finite-amplitude wave that has the frequency of the fundamental locks itself to the subharmonic and both waves start travelling at the same phase speed (Ho & Huang 1982). This results in an energy transfer to the subharmonic via a parametric resonance mechanism (Hajj *et al.* 1992).

Measurements of quantities such as phase difference, phase coupling (i.e. locking), and phase speed matching are necessary to provide the experimental counterpart for existing theories. However, under 'natural' conditions, these quantities are not constant with time and typically have large variances. A more meaningful measure of these quantities and subsequent comparison with theories can be obtained by reducing this variance through controlled excitation of the mixing layer.

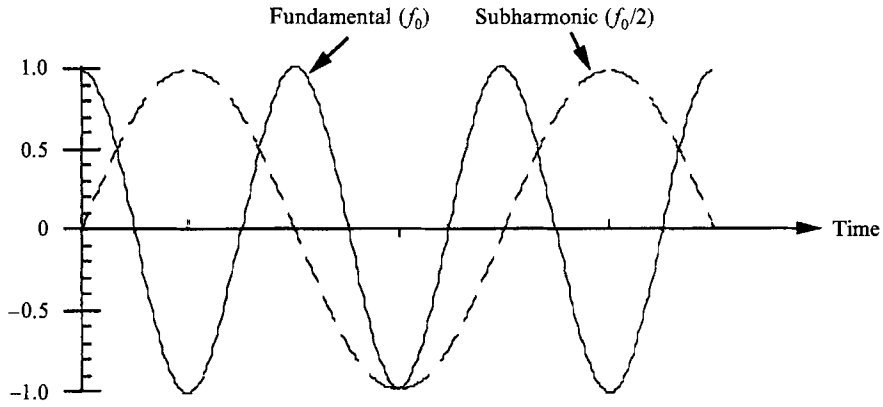

FIGURE 5. Schematic of fundamental and subharmonic modes with a phase difference

$$\Delta\Phi_0 = \Phi(f_0) - \Phi(f_0/2) = \pi/2$$

AT $t = 0$. Note that this phase difference is equal to $\Omega = \Phi(f_0) - 2\Phi(f_0/2)$ at any time t.

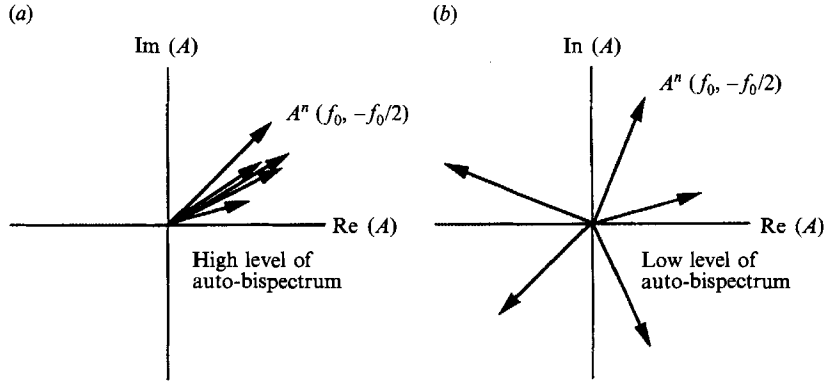

FIGURE 6. Vector representation of N estimates of the auto-bispectrum

$$A^n(f_0, -f_0/2) = X(f_0)\,X^*(f_0/2)\,X^*(f_0/2).$$

(*a*) Case of coupled modes resulting in constant phase difference and high level of auto-bispectrum. (*b*) Case of non-coupled modes resulting in random phase difference and low auto-bispectrum. $n = 1, \ldots, N$.

3.2. *Fundamental–subharmonic phase difference and coupling*

Because transition starts with a linear region where fluctuations at the fundamental and subharmonic frequencies travel at different phase speeds, the phase relation between the two modes changes with downstream distance. It is the phase relation at the onset of parametric and nonlinear interactions that determines the efficiency of energy transfer to the subharmonic. In general, because the fundamental and subharmonic modes have different frequencies, the instantaneous phase difference in a time series will vary from one instant to another. Nikitopoulos & Liu (1987) and Riley & Metcalfe (1980) chose to specify phase difference $\Delta\Phi_0$ by setting the phase of the subharmonic to zero. In this work, we will follow this convention for $\Delta\Phi_0$ and set the phase of the subharmonic to zero at $t = 0$. Figure 5 shows the case of a perfectly phase-coupled fundamental with its subharmonic where the phase difference, $\Delta\Phi_0$, at $t = 0$ is $\frac{1}{2}\pi$. Because the frequency of the fundamental is twice that of the subharmonic, the quantity Ω defined by $\Phi(f_0) - 2\Phi(f_0/2)$ will at all times be equal to the value measured at $t = 0$ and will hence yield $\Delta\Phi_0$. Therefore, a statistical average of Ω over successively

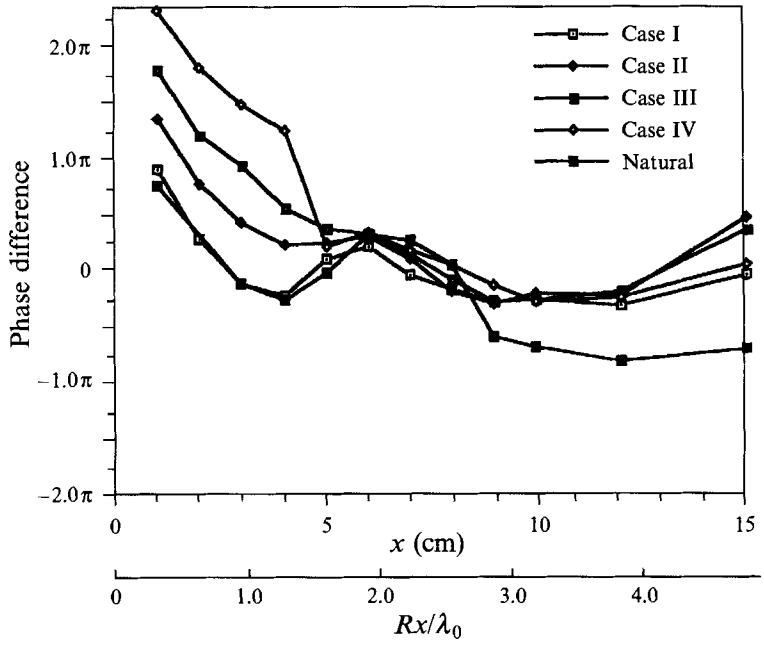

FIGURE 7. Downstream variations of the phase difference between the fundamental and subharmonic modes under the different excitation conditions.

measured records can be used as a meaningful measure of $\Delta\Phi_0$ from record to record. In the case where the coupling between the fundamental and subharmonic modes is only partial, the quantity given by Ω in any given record will be different.

A statistical measure of Ω, and thus the phase difference, $\Delta\Phi_0$, can be obtained from the phase of the auto-bispectrum, defined as $A(f_0, -f_0/2) = E[X(f_0)\, X^*(f_0/2)\, X^*(f_0/2)]$. In this definition, $X(f_0)$ and $X(f_0/2)$ are the complex Fourier transforms of the fluctuating signals at the frequencies of the fundamental and subharmonic modes and the notation $E[\ldots]$ denotes a statistical average. The auto-bispectrum is a complex quantity that can be represented as a vector (Ritz 1991). If, as shown schematically in figure 6(*a*), the phase of the auto-bispectrum vector has a small variance over many time records, the magnitude of the average vector of the auto-bispectrum is large and the three modes are highly coupled and coherent. In contrast, if, as in figure 6(*b*), the phase of the auto-bispectrum varies randomly over many records, the vector average of the auto-bispectrum will be near zero indicating that the three modes are not coupled and thus not correlated.

Kim & Powers (1979) showed that the variance of the auto-spectrum estimator is dependent on the auto-bicoherence defined as

$$b^2(f_0, -f_0/2) = \frac{|A(f_0, -f_0/2)|^2}{E[|X(f_0/2)X(f_0/2)|^2]\, E[|X(f_0)|^2]}. \tag{1}$$

Based on this, the level of confidence that can be placed in our measure of Ω is also a function of the auto-bicoherence. A value near zero indicates a random phase relation between poorly coupled fundamental and subharmonic modes and the measured Ω is irregular. A value near one indicates that the two modes are highly coupled and the measured Ω remains constant. Any value in between indicates a degree of partial coupling and determines the degree of variance of the measured Ω and hence our estimate of $\Delta\Phi_0$.

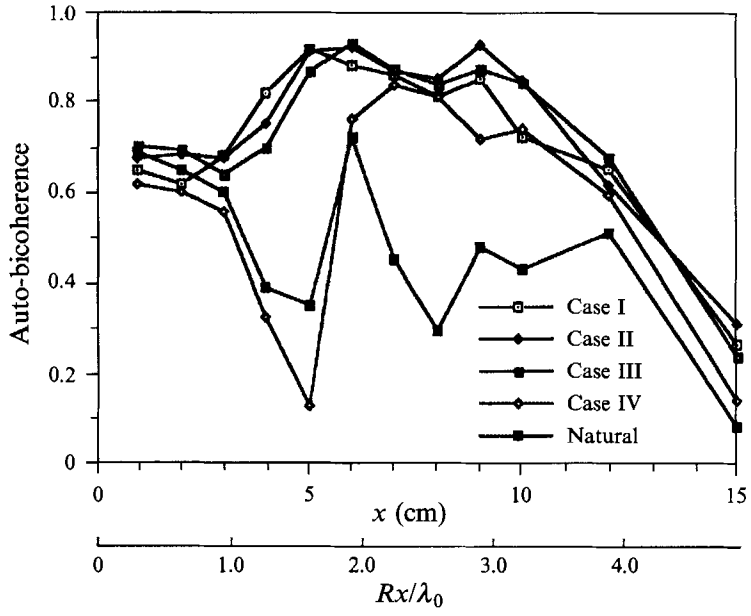

FIGURE 8. Downstream variations of the auto-bicoherence between the fundamental and the subharmonic modes under the different excitation conditions.

Figure 7 shows the variation in the measured phase difference, $\Delta\Phi_0$, in the downstream direction under 'natural' and controlled excitation conditions. At $Rx/\lambda_0 = 0.3$, the phase differences in the four phase-controlled excitations are 0.90π, 1.35π, 1.79π, and 2.32π, respectively. While, the value of the phase difference in each excitation case changes between $Rx/\lambda_0 = 0.3$ and 1.0, the roughly $\frac{1}{2}\pi$ increments between the different cases is maintained throughout this region. By $Rx/\lambda_0 = 1.3$, the phase difference between the fundamental and the subharmonic in the four cases of excitations have changed to -0.23π, 0.22π, 0.55π, and 1.24π. The level of confidence in these values, as estimated by the level of the auto-bicoherence, is shown in figure 8. The levels of coupling between the fundamental and the subharmonic in the first three cases are larger than 0.6 and 0.7, slightly larger than the values measured at $Rx/\lambda_0 = 1.0$. This indicates that, in these three cases, the fundamental and subharmonic modes are highly coupled and that the corresponding measured phase differences have a very low variance. These three cases will be considered as examples of high fundamental–subharmonic coupling and will be referred to as Cases I, II, and III. In the fourth excitation case, the phase difference at $Rx/\lambda_0 = 1.3$ is 1.24π, and figure 8 shows that the coupling level has decreased to 0.3 (low level of coupling) which indicates that the phase difference is irregular and may vary considerably from the measured value. This fourth case will be considered as an example of low fundamental–subharmonic coupling and will be referred to as Case IV.

As the transition progresses, figure 7 shows that, by $Rx/\lambda_0 = 1.6$, the phase differences in all four cases are tending towards a common value near zero. Figure 8 shows that the level of coupling between the fundamental and subharmonic maintains a high value of Cases I, II, and III and a low value in Case IV. By $Rx/\lambda_0 = 2.0$, the coupling level in Case IV increases to match those levels measured in the other three cases and the phase differences in all four cases converge to values that are near zero. Beyond $Rx/\lambda_0 = 2.0$, the variations in the phase difference in all the cases follow the

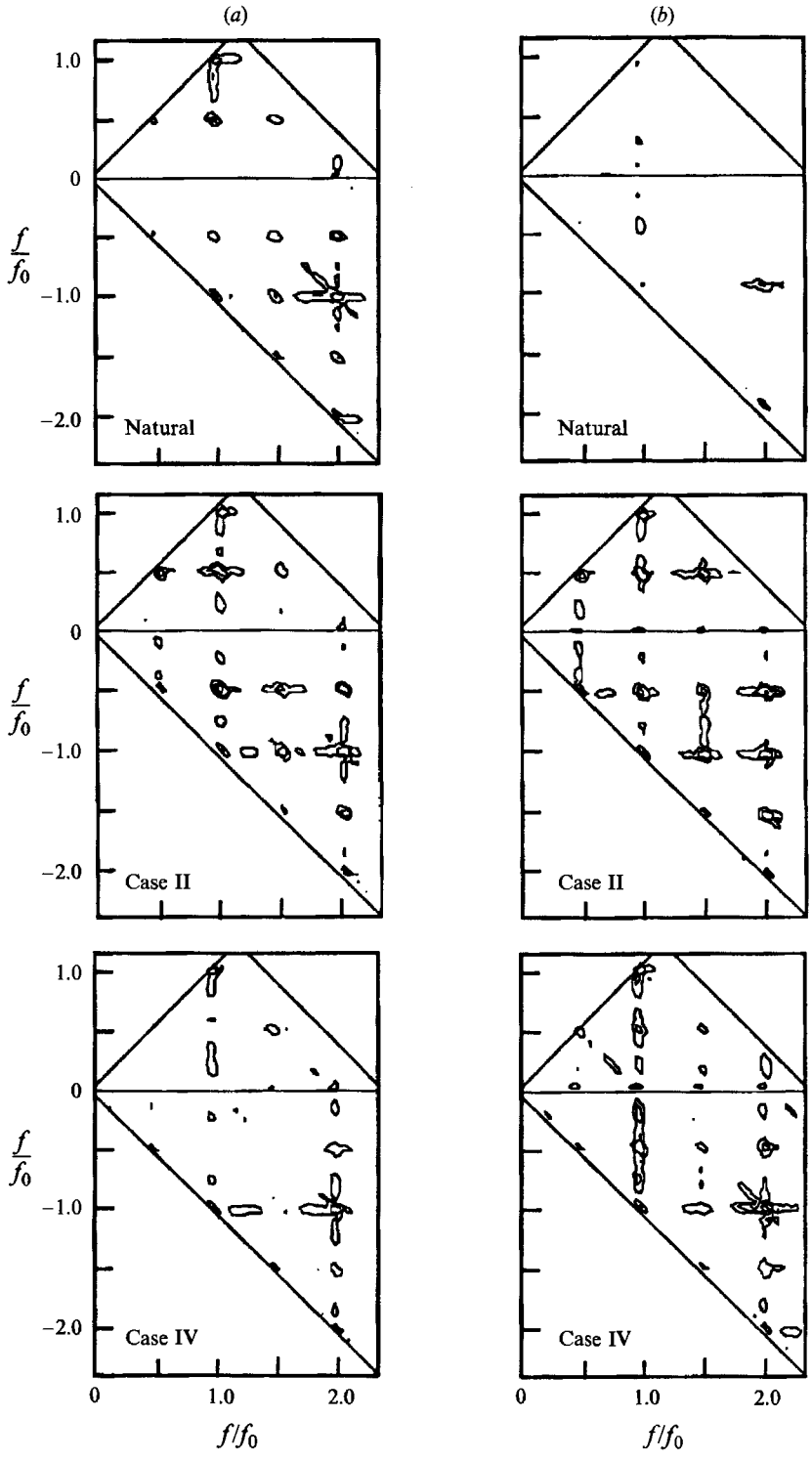

FIGURE 9. Contours of the auto-bicoherence, b^2 (f_i, f_j), under Natural, Case II, and Case IV excitations at (*a*) $Rx/\lambda_0 = 1.6$ and (*b*) 2.3. Contour levels are set at 0.3, 0.6, and 0.9.

same general behaviour. A slight decrease in the measured values of the phase difference is noted. All the measured phase differences maintain approximately constant values over distances of order of one fundamental wavelength, λ_0.

Measurements under different fundamental–subharmonic phase differences and corresponding coupling show that the basic characteristics of transition development in the downstream direction are altered, particularly in the region between $Rx/\lambda_0 = 1.3$ and 1.6. In the initial linear stage, the coupling levels between the fundamental and the subharmonic modes varied between 0.6 and 0.7 in all cases, and the roughly $\frac{1}{2}\pi$ phase increments were maintained. Between $Rx/\lambda_0 = 1.3$ and 1.6, however, the level of phase coupling between the fundamental and the subharmonic in Cases I, II, and III increased to values between 0.8 and 0.9, which are larger than the levels measured in the initial linear stage. In contrast the level of phase coupling between $Rx/\lambda_0 = 1.3$ and 1.6 in Case IV decreased. Beyond $Rx/\lambda_0 = 1.6$, the level of coupling between the fundamental and its subharmonic in Case IV increased to levels comparable with those measured in this region for the other three cases. Coupling-level measurements under 'natural' excitation conditions show a pattern similar to Case IV. By $Rx/\lambda_0 = 2.0$, the phase difference in all cases is close to zero.

In order to identify the overall effect of the fundamental–subharmonic phase relation on the mode coupling between other flow components, two-dimensional contour plots of auto-bicoherence measurements of the longitudinal fluctuations under natural, Case II, and Case IV excitations are shown in figure 9. The plots are shown at two different downstream locations, namely $Rx/\lambda_0 = 1.6$ and 2.3. These two locations demonstrate a critical feature of the role of phase coupling in the transition. At $Rx/\lambda_0 = 16$, the coupling in Case II is at a very high value (> 0.9) while in Case IV it is very low (< 0.3). By $Rx/\lambda_0 = 2.3$, the coupling level between the fundamental and its subharmonic is fairly high in all cases.

At both locations, and under all the excitation conditions, bicoherence plots exhibit peaks at (f_0, f_0) in the sum region and $(2f_0, -f_0)$ in the difference region. This indicates high coupling between the fundamental and the first harmonic. While the fundamental (f_0) – first harmonic $(2f_0)$ coupling is not effected by the different phase excitation conditions, subharmonic couplings are affected, especially at $Rx/\lambda_0 = 1.6$. Note that the coupling level between the subharmonic and the other coherent modes, f_0, $3f_0/2$ and $2f_0$, is larger in Case II than in Case IV or in the natural excitation case. At $Rx/\lambda_0 = 2.3$, the level of coupling at $(f_0, -f_0/2)$, in Case II, remains large (> 0.9). Also, the level of coupling at $(f_0, -f_0/2)$ at $Rx/\lambda_0 = 2.3$, in Case IV and under natural excitation, is larger than that at $Rx/\lambda_0 = 1.6$. This is accompanied by an increase in the coupling level between the subharmonic and the different modes, f_0, $3f_0/2$ and $2f_0$.

3.3. *Downstream development of the spectral components – phase-controlled transition*

The downstream development of the u'_{rms} amplitudes of the fundamental and subharmonic modes, under the four different cases of phase-controlled excitation discussed above, are shown in figures 10(*a*) and 10(*b*), respectively. Both figures show that, in all cases, the growth of these two modes in the initial region up to $Rx/\lambda_0 = 1.0$ follows the same behaviour. The measured non-dimensional growth rates $\alpha\theta_0/R$ of the fundamental varied between 0.096 and 0.10 under all excitation cases. Those of the subharmonic varied between 0.050 and 0.052. These values are in agreement with those predicted by the linear spatial theory of Monkewitz & Huerre (1982). The region up to $Rx/\lambda_0 = 1.0$ will be referred to as the linear instability region.

For all cases, figure 10(*a*) shows that the fundamental starts to saturate at $Rx/\lambda_0 = 1.3$. Also, the variations in the amplitude of the fundamental in the downstream

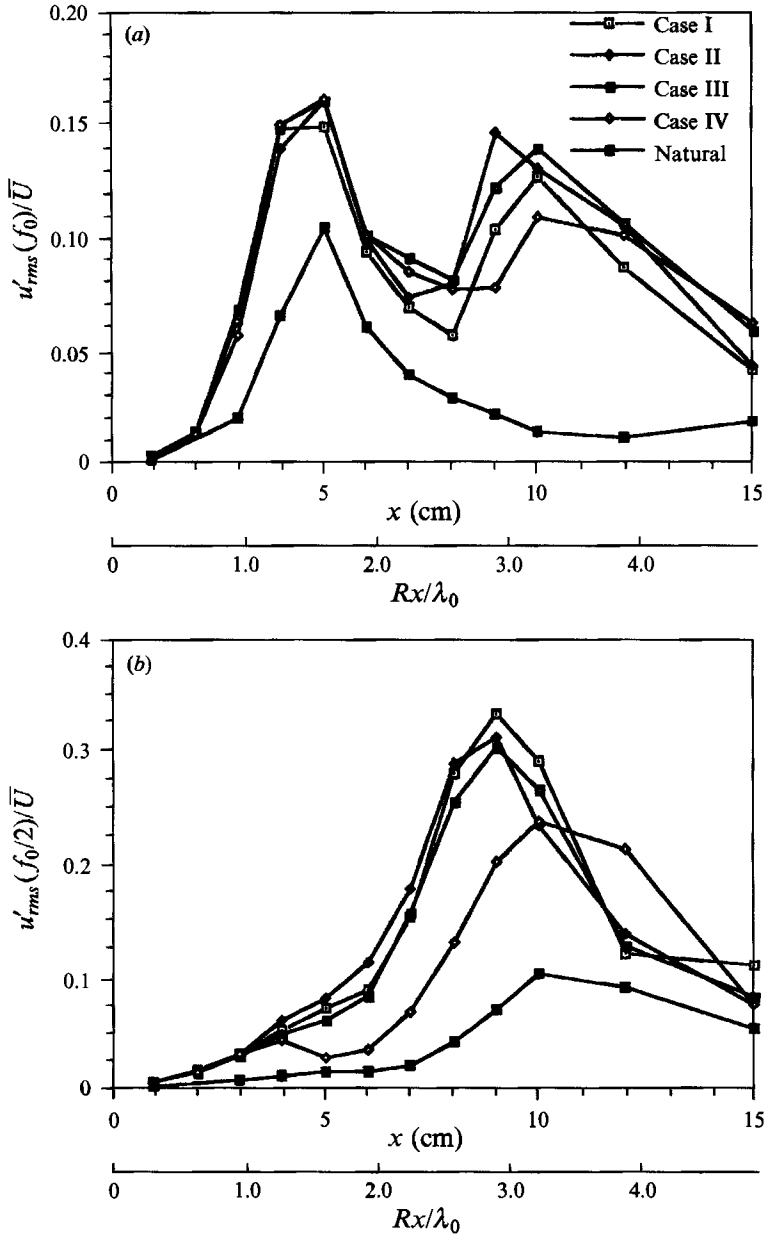

FIGURE 10. Downstream development of (*a*) the fundamental mode and (*b*) the subharmonic mode under the different excitation conditions.

direction beyond this point are similar under all the phase-controlled excitation conditions. Figure 11 shows that the subharmonic starts to deviate from exponential growth at the same position where the fundamental starts to saturate, i.e. at $Rx/\lambda_0 = 1.3$. This location will be referred to as the location where the onset of fundamental–subharmonic mode interaction starts, and the increments in phase difference between the four cases departs from $\frac{1}{2}\pi$, see figure 7. In contrast to the downstream development of the fundamental amplitude, the subharmonic amplitude

variations in the downstream direction, beyond $Rx/\lambda_0 = 1.3$, are dependent on its phase relation with the fundamental. When the flow is excited, in Cases I, II, and III, where the coupling level is high and where the phase difference is close to zero, the subharmonic continues to grow beyond $Rx/\lambda_0 = 1.3$ to achieve saturation at $Rx/\lambda_0 = 2.9$. This indicates that the exponential growth of the subharmonic in Cases I, II, and III is followed directly by an efficient mechanism for the transfer of energy to the subharmonic. On the other hand, when the flow is excited in Case IV, where the coupling level is very low between $Rx/\lambda_0 = 1.3$ and 1.6, the subharmonic growth is suppressed. However, at $Rx/\lambda_0 = 2.0$, where the coupling level between the fundamental and the subharmonic in Case IV increases to match the high levels of Cases I, II, and III and where the phase difference is near zero, the subharmonic amplitude resumes its growth and finally saturates at $Rx/\lambda_0 = 3.2$, at a level some 35% smaller than that observed in Cases I, II, and III. The subharmonic growth in Case IV comes closest to matching that observed under the natural conditions.

3.4. *Fundamental–subharmonic phase-speed matching*

Hajj *et al.* (1992) showed that the growth of the subharmonic beyond the initial linear region is controlled by a parametric interaction between the fundamental and the subharmonic. The region of subharmonic growth in Cases I, II, and III, between $Rx/\lambda_0 = 1.3$ and 2.9, will be referred to as the parametric region of subharmonic growth. In Case IV, subharmonic growth is suppressed at $Rx/\lambda_0 = 1.3$ and 1.6 before it resumes to grow beyond $Rx/\lambda_0 = 2.0$. In this case, the parametric region of subharmonic growth in Case IV starts at $Rx/\lambda_0 = 2.0$ and continues up to $Rx/\lambda_0 = 3.2$. A comparison of the values of the fundamental–subharmonic phase difference in the regions of parametric subharmonic growth indicates that a *critical phase difference* roughly equal to zero exists for maximum subharmonic growth via parametric resonance. Similar behaviour is obtained in the numerical analysis of Riley & Metcalfe (1980). Parametric resonance models suggested by Kelly (1967) for a temporally developing free shear layer, and by Monkewitz (1988) for a spatially developing free shear layer require that phase locking or synchronization is satisfied for efficient interactions to take place. In the experiments reported here, the extent of downstream phase-speed matching was determined by measuring the local phase speeds of the fundamental and subharmonic modes.

Beall, Kim & Powers (1982) devised a technique to estimate the local wavenumber/frequency spectrum, $\tilde{S}(k,f)$. This quantity provides a measurement of the local power spectrum of the fluctuations as a function of frequency f and wavenumber k. From $\tilde{S}(k,f)$, one can estimate the local dispersion relation and examine phase-speed matching conditions. In most transitioning flows, the relation between frequency f and wavenumber k, and subsequently the dispersion relation $k(f)$, is not purely deterministic. $\tilde{S}(k,f)$ will yield a band of wavenumbers associated with a given frequency and a simple measurement of phase-speed matching conditions is not possible. In addressing this problem, we have taken the approach that the fundamental–subharmonic interaction process will be dominated by the narrow bands of wavenumbers that contain most of the f_0 and $f_0/2$ energy. A measure of phase velocity at frequency f that weights the phase speed by the energy of the wavenumber associated with that frequency, can be obtained by weighting the ratio $2\pi f/k$ by the joint spectral density function, $s(k,f)$:

$$C_r(f) = \sum_k \frac{2\pi f}{k} s(k,f), \tag{2}$$

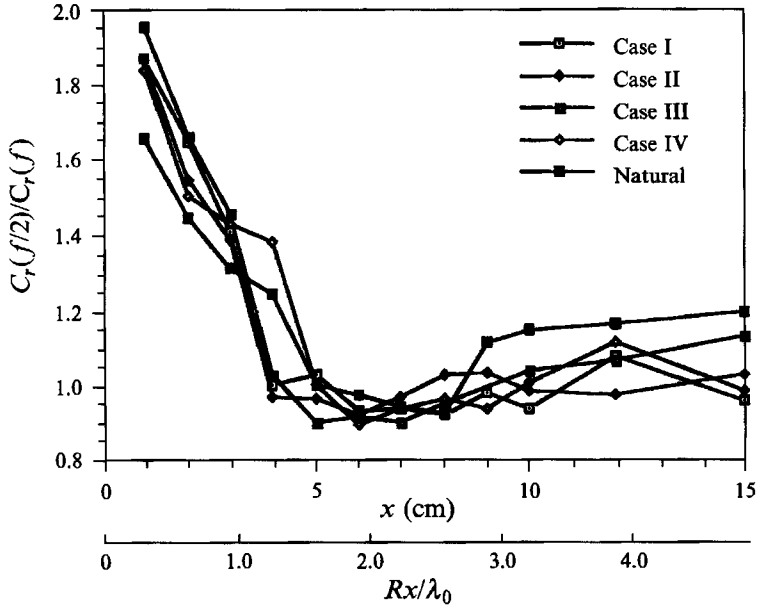

FIGURE 11. Downstream development of the phase-speed ratio, $C_r(f_0)/C_r(f_0/2)$, of the fundamental and subharmonic modes under the different excitation conditions.

where the joint spectral density function is a normalized value of $\tilde{S}(k,f)$ and is given as

$$s(k,f) = \frac{\tilde{S}(k,f)}{\sum\limits_{k;f} \tilde{S}(k,f)}. \tag{3}$$

Figure 11 shows the measured variations in the ratio of the phase speeds of the subharmonic to the fundamental in the downstream direction. In the linear instability region of the transition, between $Rx/\lambda_0 = 0.33$ and 1.0, in Cases I, II, and III the ratio of the phase speeds of the subharmonic to the fundamental, $C_r(f/2)/C_r(f)$, varies between 1.9, at $Rx/\lambda_0 = 0.33$, and 1.4 at $Rx/\lambda_0 = 1.0$. Further downstream, at $Rx/\lambda_0 = 1.3$, the ratio decreases at 1.0. At this location, in Cases I, II, and III the coupling levels between the three modes are larger than 0.8 (figure 8), the phase difference is near zero (figure 7), and the subharmonic growth rate is maximum (figure 10*b*). The ratio of the subharmonic phase speed to that of the fundamental varies between 0.9 and 1.0 in the region between $Rx/\lambda_0 = 1.3$ and 3.2, i.e. over the parametric region of subharmonic growth, indicating that the subharmonic is travelling with a phase speed that is slightly smaller than that of the fundamental.

In Case IV, the initial variation of the phase-speed ratio between $Rx/\lambda_0 = 0.33$ and 1.0, is similar to that in Cases I, II, and III. However, at $Rx/\lambda_0 = 1.3$, the ratio is not equal to unity as in Cases I, II, and III. At this location the phase coupling between the two modes is low (figure 8), and the subharmonic growth is suppressed (figure 10*b*). Further downstream, and particularly between $Rx/\lambda_0 = 2.0$ and 3.2, the region where subharmonic growth resumes (figure 10*b*), the ratio of the phase speeds approaches unity. In effect, the parametric resonance is delayed until the phase-speed matching condition is achieved. The variations in the ratio of the phase speeds of the subharmonic and fundamental modes under the natural conditions are similar to those of Case IV.

3.5. *Effect of phase relation on energy transfer rates to the subharmonic*

3.5.1. *Modelling of energy transfer rates to the subharmonic*

Hajj *et al.* (1992) described a technique for measuring local values of energy transfer due to linear, parametric, and nonlinear (quadratic) mechanisms. The relation between the velocity fluctuations at two separated but closely spaced sensors was modelled as an input–output system related by linear and interaction transfer functions of the form

$$E[Y(f_m)\,X^*(f_m)] = L(f_m)\,E[X(f_m)\,X^*(f_m)] + \sum_{f_i \pm f_j = f_m} I^{f_m}_{f_i;f_j}\,E[X(f_i)\,X(f_j)\,X^*(f_m)], \quad f_m = f_i \pm f_j, \tag{4}$$

where the left-hand side represents the cross-power spectrum. The first term on the right-hand side models the *linear* contribution to the cross-spectrum from the auto-spectrum at the upstream sensor at the same frequency component f_m. The second term models *interactions* between the f_i and f_j components at the upstream sensor that contribute to the cross-spectrum at the f_m component. For the particular case of the fundamental–subharmonic interaction (i.e. when $f_m = f_0/2$, $f_i = f_0$ and $f_j = f_0/2$), (4) becomes

$$E[Y(f_0/2)\,X^*(f_0/2)] = L(f_0/2)\,E[X(f_0/2)\,X^*(f_0/2)] + I^{f_0/2}_{f_0;f_0/2}\,E[X(f_0)\,X(f_0/2)\,X^*(f_0/2)]. \tag{5}$$

When the fundamental and subharmonic components interact *nonlinearly*, energy transfer takes place between the fundamental and the subharmonic and the amplitude of both modes vary. In contrast, when the interaction is *parametric*, variations in the subharmonic component will not affect the fundamental mode and $X(f_0)$ can then be treated as a constant. The interaction term can then be divided into parametric and nonlinear quadratic parts, such as

$$I^{f_0/2}_{f_0;f_0/2}\,E[X(f_0)\,X(f_0/2)\,X^*(f_0/2)] = X(f_0)\,P^{f_0/2}_{f_0;f_0/2}\,E[X(f_0/2)\,X^*(f_0/2)] + Q^{f_0/2}_{f_0;f_0/2}\,E[X(f_0)\,X(f_0/2)\,X^*(f_0/2)]. \tag{6}$$

The first term in (6) models parametric interactions and the second term represents nonlinear quadratic interactions. For parametric interactions $X(f_0)$ can be treated as a constant (Kelly 1967), and thus is taken outside the expected value, demonstrating the linear-like behaviour of parametric effects. Equation (5) can then be rewritten as

$$E[Y(f_0/2)\,X^*(f_0/2)] = L_e(f_0/2)\,E[X(f_0/2)\,X^*(f_0/2)] + Q^{f_0/2}_{f_0;f_0/2}\,E[X(f_0)\,X(f_0/2)\,X^*(f_0/2)], \tag{7}$$

where $L_e(f_0/2)$ is defined as an 'effective' linear transfer function, which includes both linear and parametric effects and has the following form:

$$L_e(f_0/2) = L(f_0/2) + X(f_0)\,P^{f_0/2}_{f_0;f_0/2}. \tag{8}$$

The dependence of the parametric energy transfer on the complex Fourier transform at the fundamental frequency in our model is consistent with the analyses of Kelly (1967) and Monkewitz (1988). As shown by Ritz, Powers & Bengtson (1989), the transfer functions defined in (7) are related to more physically meaningful variables such as the growth rates, dispersion relation and quadratic three-wave coupling coefficients. In the case of the subharmonic component, the effective complex linear transfer function, $L_e(f_0/2)$, is given by

$$L_e(f_0/2) = [(\alpha_e(f_0/2) + \mathrm{i}k_e(f_0/2))\,\Delta x + 1 - \mathrm{i}\Delta\Theta(f_0/2)]\,\mathrm{e}^{\mathrm{i}\Delta\Theta(f_0/2)}. \tag{9}$$

In this equation, $\Delta\Theta(f_0/2)$ is the phase shift of the subharmonic mode between the two sensors, $\alpha_e(f_0/2)$ is the 'effective' linear growth rate, and $k_e(f_0/2)$ is the 'effective' dispersion relation. The complex function $1-i\Delta\Theta(f_0/2)$ accounts for the advection of the subharmonic mode from the upstream to the downstream sensor. The effective linear growth rate, $\alpha_e(f_0/2)$, includes the linear as well as the parametric effects and, based on (8), can be written as

$$\alpha_e(f_0/2) = \alpha_l(f_0/2)+\alpha_p(f_0/2), \tag{10}$$

where $\alpha_l(f_0/2)$ and $\alpha_p(f_0/2) = \mathrm{Re}[X(f_0)\, P^{f_0/2}_{f_0/2;f_0/2}]$ are the exponential and parametric growth rates respectively.

Ritz & Powers (1986) and Kim & Powers (1988) present two different methods for estimating the linear and quadratic transfer functions given in (7). Based on these methods, Hajj *et al.* (1992) quantified the energy transfer rates between the two sensors of the probe by an energy transfer relation of the form:

$$\Delta S(f_m) = S'_L(f_m)+S_Q(f_m)+S_{LQ}(f_m), \tag{11}$$

where $\Delta S(f_m) = \hat{S}_{yy}(f_m)-S_{xx}(f_m)$ is the difference in energy measured between the upstream and downstream sensors of the probe. The detailed relations between these transfer rates and the linear and quadratic transfer functions are given by Hajj *et al.* (1992). $S'_L(f_m)$ accounts for that part of the difference that is due to linear and parametric mechanisms, $S_Q(f_m)$ accounts for the part due to nonlinearly quadratic mechanisms, and $S_{LQ}(f_m)$ is referred to as linear–quadratic energy transfer because it includes both transfer functions. $S_{LQ}(f_m)$ is a result of the non-Gaussian property of the input signal and thus includes an upstream memory factor. In order to determine local energy transfer characteristics, $S_{LQ}(f_m)$ must be minimized. Recently, Kim *et al.* (1991) presented a minimum mean-square error estimation technique that allows the linear–quadratic term, $S_{LQ}(f_m)$, to be eliminated. The effective linear and quadratic transfer functions are determined from the following equations:

$$L_e(f_m) = E[Y(f_m)\, X^*(f_m)]/E[X(f_m)\, X^*(f_m)] \tag{12}$$

and

$$\sum_{f_i\pm f_j=f_m}\sum_{f_k\pm f_l=f_m} Q^{f_m}_{f_i;f_j}\, E[X^*(f_i)\, X^*(f_j)\, X(f_k)\, X(f_l)]$$
$$= E[(Y(f_m)-L_e(f_m)\, X(f_m))\, X^*(f_i)\, X^*(f_j)], \tag{13}$$

where $f_m = f_i\pm f_j = f_k\pm f_l$. From these estimates of $L_e(f_m)$ and $Q^{f_m}_{f_i;f_j}$, one can quantify the total energy transfer rate, $T_{tot}(f_m) = \Delta S(f_m)/\Delta x$ as

$$T_{tot}(f_m) = T_{L_e}(f_m)+T_Q(f_m), \tag{14}$$

where the 'effective' linear energy transfer rate is given by

$$T_{L_e}(f_m) = 2\alpha_e(f_m)\, E[X(f_m)\, X^*(f_m)] \tag{15}$$

and the nonlinear quadratic energy transfer rate, $T_Q(f_m)$, is given by

$$T_Q(f_m) = \sum_{f_k\pm f_l=f_m} (T_Q)^{f_m}_{f_k;f_l}$$
$$= \sum_{f_k\pm f_l=f_m} Q^{f_m *}_{f_k;f_l} \sum_{f_i\pm f_j=f_m} Q^{f_m}_{f_i;f_j}\, E[X^*(f_k)\, X^*(f_l)\, X(f_i)\, X(f_j)]/\Delta x. \tag{16}$$

In the above equations, Δx denotes the streamwise separation between the two sensors.

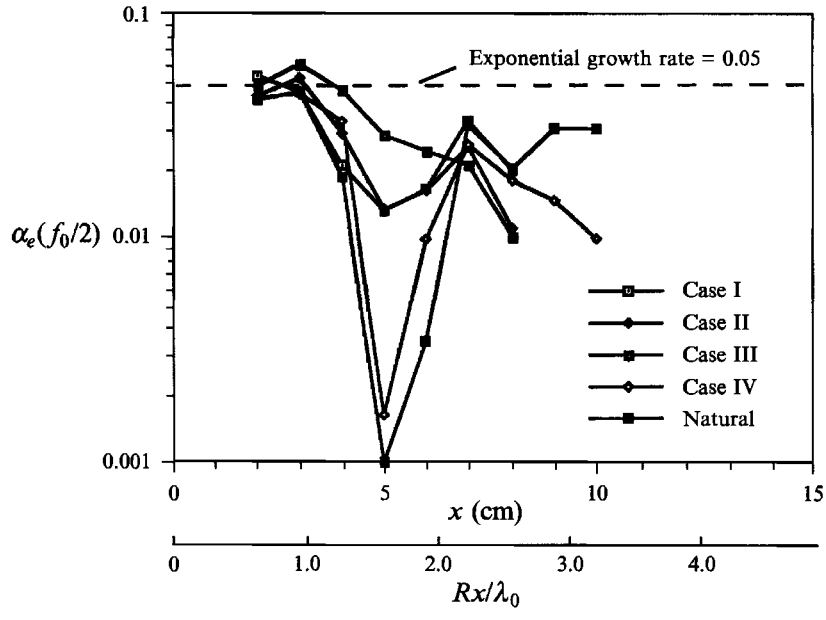

FIGURE 12. Downstream development of the effective linear growth rate of the subharmonic mode, $\alpha_e(f_0/2)$, under the different excitation conditions.

For the case of the fundamental–subharmonic interaction, the 'effective' linear energy transfer rate, $T_{L_e}(f_0/2)$, is given by

$$\begin{aligned} T_{L_e}(f_0/2) &= 2\alpha_e(f_0/2)\,E[X(f_0/2)\,X^*(f_0/2)] \\ &= 2\{\alpha_i(f_0/2)\,E[X(f_0/2)\,X^*(f_0/2)] + \mathrm{Re}\,[P^{f_0/2}_{f_0;f_0/2}\,E[X(f_0)\,X(f_0/2)\,X^*(f_0/2)]]\}, \end{aligned} \tag{17}$$

where the linear and parametric energy transfer are represented by the first and second terms in the brackets, respectively. Note that strictly speaking, the second term of (17) involves the difference interaction of the form $f_0 - f_0/2 = f_0/2$. Note also the dependence of the parametric energy transfer on the complex Fourier transform at the fundamental frequency. This shows the importance of the fundamental amplitude and its phase relation with the subharmonic for parametric energy transfer.

3.5.2. *Estimates of energy transfer rates to the subharmonic*

Estimates for linear and quadratic energy transfer rates given in (16) and (17) were used to investigate two mechanisms put forward by Kelly (1967) for subharmonic growth beyond the linear instability region. In Kelly's first mechanism, a periodic component of the mean flow that originates from the fundamental mode and therefore is characterized by its frequency and wave number interacts with a disturbance to reinforce another disturbance. In this case, the periodic component will interact with the 3/2 harmonic to reinforce the subharmonic and vice versa. This mechanism is similar to the three-wave resonance phenomenon discussed by Raetz (1959) and is a part of equation (16) in our model. In Kelly's second mechanism, the periodic component set up by the fundamental interacts with a disturbance at the subharmonic frequency to reinforce the energy at the subharmonic. This mechanism is basically a parametric resonance phenomenon and appears as a part of the energy transfer rate given in equation (17). Estimates of the effective linear growth rate of the subharmonic,

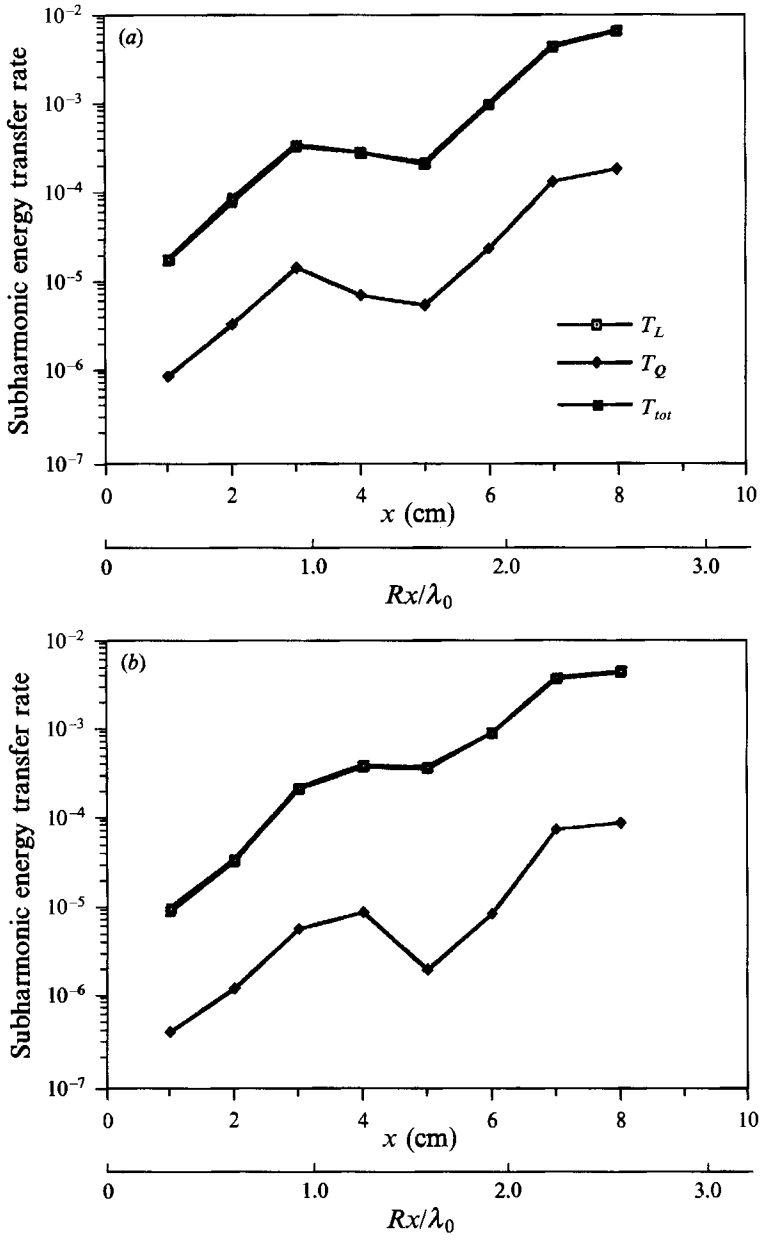

FIGURE 13(*a*, *b*). For caption see facing page.

$\alpha_e(f_0/2)$, for the different cases of excitation, are given in figure 12. Note that in all cases, the measured effective linear growth rates, $\alpha_e(f_0/2) = \frac{1}{2}T_{L_e}(f_0/2)/S_{xx}(f_0/2))$, up to $Rx/\lambda_0 = 1.0$, are close to 0.05 (1/mm) which falls close to the measured values obtained by assuming exponential growth and determined based on the relation $\alpha_l(f_0/2) = (1/\Delta x)\ln[|Y(f_0/2)|^2/|X(f_0/2)|^2]^{.5}$. This shows that, in this initial region, the growth of the subharmonic component is independent of any interaction mechanisms with the fundamental. Beyond this initial instability region, the measured effective linear growth rate shows different values under the different cases of phase-controlled excitations.

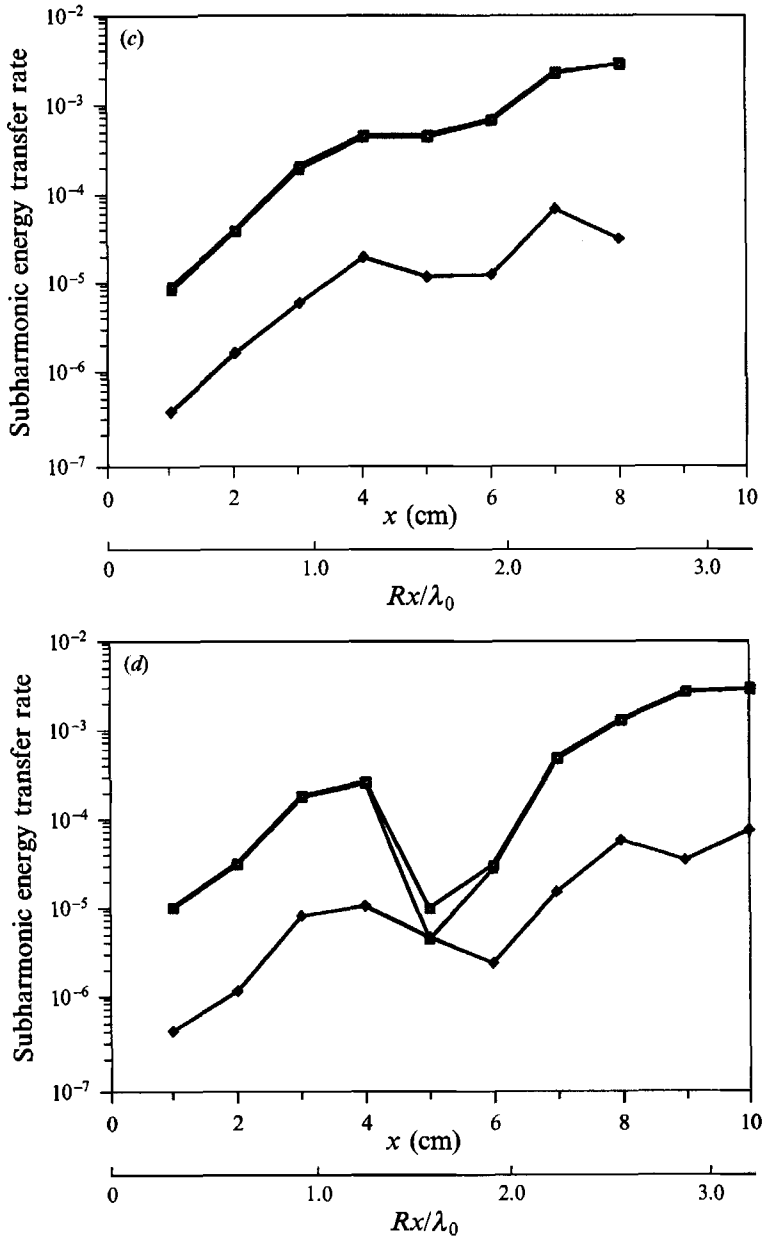

FIGURE 13. Downstream variations of the linear, $T_{L_e}(f_0/2)$, quadratic, $T_Q(f_0/2)$, and total, $T_{tot}(f_0/2)$, energy transfer rates to the subharmonic for (*a*) Case I, (*b*) Case II, (*c*) Case III, and (*d*) Case IV excitation.

In Cases I, II, and III, where the coupling level between the fundamental and the subharmonic is large (figure 8), and where the phase difference between the two modes is close to zero (figure 7), the growth rate in the parametric region of subharmonic growth has the same order of magnitude as that measured in the linear instability region up to $Rx/\lambda_0 = 1.0$. In Case IV, at $Rx/\lambda_0 = 1.6$, where the coupling between the two modes is low (figure 8) and where the phase difference is not constant, the growth rate sharply decreases to slightly less than two orders of magnitude below that

	$Rx/\lambda_0 = 0.3$		$Rx/\lambda_0 = 1.3$	
Cases	$\Phi(f_0)-2\Phi(f_0/2)$	$b^2(f_0,f_0/2)$	$\Phi(f_0)-2\Phi(f_0/2)$	$b^2(f_0,f_0/2)$
I	0.90π	0.65 (high)	-0.23π	0.82 (high)
II	1.35π	0.68 (high)	0.21π	0.75 (high)
III	1.79π	0.70 (high)	0.55π	0.70 (high)
IV	2.32π	0.62 (high)	1.24π	0.32 (low)
Natural	0.74π	0.69 (high)	-0.27π	0.39 (low)

TABLE 1. Phase difference and coupling characteristics between the fundamental and subharmonic modes at two downstream locations

measured in Cases I, II and III, and the growth of the subharmonic is suppressed (figure 10*b*). The same behaviour is observed under the natural conditions. Further downstream, as the subharmonic resumes its growth at $Rx/\lambda_0 = 2.0$, the level of linear growth rate increases to levels comparable with those measured in Cases I, II and III. This increase is maintained up to $Rx/\lambda_0 = 3.2$.

The variations in the downstream direction of the relative levels of the linear, quadratic and total energy transfer rates to the subharmonic component, in Cases I, II, III and IV are shown in figures 13(*a*)–13(*d*), respectively. In the initial region of the subharmonic growth, up to $Rx/\lambda_0 = 1.0$, the linear energy transfer rate increases exponentially in all cases, which shows that the subharmonic growth in this region is governed by a linear instability mechanism. Further downstream, the linear energy transfer rate, $T_{L_e}(f_0/2)$, in Cases I, II, and III, is always larger than the quadratic energy transfer rate, $T_Q(f_0/2)$. The energy increase of the subharmonic component in these Cases (figure 10*b*), indicates the importance of linear-like mechanisms, such as the parametric mechanism, in the energy transfer to the subharmonic.

Figure 13(*d*) shows that while the quadratic energy transfer rate in Case IV is of the same order as that observed in Cases I, II, and III, the linear energy transfer rates decrease sharply between $Rx/\lambda_0 = 1.3$ and 1.6. By comparison with figure 10(*b*) it is noted that the suppression of subharmonic growth in this region is largely due to the sharp decrease in the linear energy transfer rate. This suggests that parametric energy transfer is not particularly efficient in this region. Further downstream, between $Rx/\lambda_0 = 2.0$ and 3.2, the linear energy transfer rate increases (figure 13*d*) and is accompanied by a growth of the subharmonic component (figure 10*b*), indicating that the efficiency of the parametric mechanism in transferring energy to the subharmonic has increased.

4. Discussion

The above measurements show that by exciting the flow at the fundamental and subharmonic modes at different relative phases, the downstream characteristics of the phase difference and coupling between the fundamental and subharmonic are altered, as seen in figures 7 and 8. Table 1 shows the different characteristics at two downstream locations. The first, at $Rx/\lambda_0 = 0.32$, is in the linear instability region. The second, at $Rx/\lambda_0 = 1.3$, marks the end of the region of exponential growth and the onset of the parametric and nonlinear activities. The effects of the phase relation (i.e. difference and coupling) between the fundamental and the subharmonic, such as those given in table 1, on the growth of the subharmonic are considered.

The downstream development of the fundamental mode, shown in figure 10(*b*),

Case	$Rx/\lambda_0 = 1.6$ $\Phi(f_0)-2\Phi(f_0/2)$	$Rx/\lambda_0 = 1.6$ $b^2(f_0,f_0/2)$	Subharmonic growth at $Rx/\lambda_0 = 1.6$	Parametric energy transfer rate at $Rx/\lambda_0 = 1.6$	Phase speed ratio $C_r(f/2)/C_r(f)$ at $Rx/\lambda_0 = 1.3$
I	0.089π	0.92 (high)	continuous	0.027	0.99
II	0.244π	0.91 (high)	continuous	0.028	0.96
III	0.374π	0.87 (high)	continuous	0.060	1.02
IV	0.203π	0.13 (low)	suppressed	0.003	1.37
Natural	-0.039π	0.35 (low)	suppressed	0.002	1.24

TABLE 2.

Case	$Rx/\lambda_0 = 2.0$ $\Phi(f_0)-2\Phi(f_0/2)$	$Rx/\lambda_0 = 2.0$ $b^2(f_0,f_0/2)$	Subharmonic growth at $Rx/\lambda_0 = 2.0$	Parametric energy transfer rate at $Rx/\lambda_0 = 2.0$	Phase speed ratio $C_r(f/2)/C_r(f)$ at $Rx/\lambda_0 = 2.0$
IV	0.17π	0.84 (high)	resumed	0.053	0.932
Natural	0.22π	0.43 (moderate)	resumed	0.065	0.940

TABLE 3.

shows a very weak dependence on its phase relation with the subharmonic. In contrast, the growth of the subharmonic, beyond the initial region of linear instability, is distinctly influenced by its changing phase relation with the fundamental as shown in figure 11. In Cases I, II, and III, where the coupling levels are large and the phase differences approach zero as the linear stage of transition comes to an end at $Rx/\lambda_0 = 1.3$, subharmonic growth is continuous. In contrast, in Case IV, where the phase coupling levels between the two modes are low at the end of the linear instability region, subharmonic growth is suppressed for roughly one wavelength of downstream distance. Further downstream, as the level of coupling between the two modes in Case IV again increases, and the phase difference approaches zero, the subharmonic mode resumes its growth just as observed in Cases I, II, and III.

These results indicate that a reduction in the coupling level between the fundamental and the subharmonic results in a suppression of subharmonic growth and that in all cases maximum amplification of the subharmonic takes place at a *critical phase difference* that is close to zero. Monkewitz (1988) showed that the reduction in the subharmonic growth rate over a substantial region and its later amplification further downstream takes place for certain fundamental–subharmonic phase relation and fundamental amplitude. Monkewitz suggested that the reduction in the subharmonic growth rate is related to the shredding mechanism observed in the numerical studies of Riley & Metcalfe (1980) and Patnaik *et al.* (1976). This indicates that our Case IV may correspond to the 'shredding' behaviour.

Measurements of the local wavenumber and phase speeds of the subharmonic and fundamental show that when the coupling between the fundamental and subharmonic modes is high, and when the phase difference is close to zero, the condition of matching phase speeds required for spatial resonance between the two modes is satisfied, table 2. This matching is maintained over the region where the subharmonic gains energy, figure 7. In contrast, when the phase coupling is low and the phase difference is irregular, the phase speed matching condition is not met and subharmonic growth is suppressed, table 2. The delay in achieving phase speed matching conditions observed in Case IV is also observed in the natural excitation case, see Hajj *et al.* (1992). This is in basic agreement with the analytical studies of Kelly (1967) and Monkewitz (1988)

which require phase-speed matching as a condition for efficient energy transfer. It is important to note here that because the subharmonic is spatially growing, any significant energy transfer requires that resonant coupling (i.e. phase speed matching) takes place over a spatial streamwise interval. The results presented here show that while the phase-speed ratio varies from one location to another, the phase-speed matching requirement is satisfied over streamwise distances of the order of the wavelength of the fundamental mode, λ_0, which is equal to 1.98 cm in this case.

The influence of the fundamental–subharmonic phase relation on subharmonic growth was also investigated to determine its effect on the parametric mechanisms responsible for transfer of energy to the subharmonic (Hajj *et al.* 1992). Table 2 shows that in regions where coupling between the two modes is low, the level of parametric energy transfer is low. When the coupling level between the two modes is large and the phase difference is equal to zero, the parametric transfer of energy is high, table 3. The results also show that the fundamental–subharmonic quadratic power transfer rates are negligible in comparison with the quasi-linear parametric energy transfer. The growth of the subharmonic beyond the region of linear instability is clearly the result of parametric resonance energy transfer to the subharmonic, regardless of the initial phase conditions, in all cases studied here, both natural and controlled.

A comparison of subharmonic growth and related energy transfer mechanisms under different phase-controlled and natural transition conditions suggests that Case IV comes closest to matching natural transition behaviour as defined by subharmonic growth (figure 10*a*), coupling characteristics (figure 8) and energy transfer measurements (figure 12). In both natural and Case IV excitation cases, the drop in the coupling level is accompanied by a suppression of the subharmonic growth at the onset of parametric interaction. This indicates that perfect subharmonic growth and phase coupling, as required for maximum subharmonic growth according to theory, does not take place under the natural conditions. This is not surprising as each tunnel has its own background excitation field that sets the initial conditions for so-called 'natural' transition and these phase conditions and coupling must be determined before a meaningful comparison of natural experiments can be made with theory.

5. Conclusions

The results presented here show that subharmonic growth is dependent on its local phase relation with the fundamental. When phase coupling between the fundamental and subharmonic modes is high and when the phase difference is close to zero, the two modes travel at the same phase speed and parametric energy transfer to the subharmonic is efficient. This results in the subharmonic gaining energy and continuing its growth beyond the linear instability region. In contrast, when the coupling between the fundamental and subharmonic modes is low and the phase difference between the two modes is irregular, parametric energy transfer is not efficient and spatial resonance matching conditions are not met. This results in a suppression of the subharmonic growth beyond the linear instability region until, further downstream, the coupling level increases and the phase difference approaches zero. Then, the fundamental and subharmonic modes start to travel at the same phase speed and parametric energy transfer becomes efficient enough for the subharmonic to resume its growth. Based on these results, we conclude that maximum subharmonic growth via parametric resonance takes place at a *critical phase difference* close to zero. The results show qualitative agreement with the numerical work of Riley & Metcalfe (1980) and the theoretical analyses of Kelly (1967) and Monkewitz (1988).

The authors wish to thank C. P. Ritz for numerous and valuable discussions. This work is based in part upon work supported by the Texas Advanced Research Program under Grant No. ARP 3280, and in part by the National Science Foundation under Grant No. MSM-8211205. The digital signal processing techniques were developed under the auspices of the Department of Defense Joint Services Electronics Program under the Air Force Office of Scientific Research (AFOSR) Contract No. F49620-89-C-0044.

REFERENCES

ARBY, H. & FFOWCS WILLIAMS, J. D. 1984 Active cancellation of pure tones in an excited jet. *J. Fluid Mech.* **149**, 445–454.

BEALL, J. M., KIM, Y. C. & POWERS, E. J. 1982 Estimation of wavenumber and frequency spectra using fixed probe pairs. *J. Appl. Phys.* **53**, 3933–3940.

FREYMUTH, P. 1966 On transition in a separated laminar boundary layer. *J. Fluid Mech.* **25**, 683–704.

HAJJ, M. R. 1990 An experimental investigation of the nonlinear interactions associated with the subharmonic growth in a plane mixing layer. PhD dissertation, The University of Texas at Austin.

HAJJ, M. R., MIKSAD, R. W. & POWERS, E. J. 1991 Experimental investigation of the fundamental-subharmonic coupling: effect of the initial phase difference. *AIAA Paper* 91-0624.

HAJJ, M. R., MIKSAD, R. W. & POWERS, E. J. 1992 Subharmonic growth by parametric resonance. *J. Fluid Mech.* **236**, 385–413.

HO, C. M. & HUANG, L. S. 1982 Subharmonics and vortex merging in mixing layers. *J. Fluid Mech.* **119**, 443–473.

HO, C. M., ZOHAR, Y., FOSS, J. K. & BUELL, J. C. 1991 Phase decorrelation of coherent structures in a free shear layer. *J. Fluid Mech.* **230**, 319–337.

HUANG, L. S. & HO, C. M. 1990 Small-scale transition in a plane mixing layer. *J. Fluid Mech.* **210**, 475–500.

JONES, F. L., RITZ, C. P., MIKSAD, R. W., POWERS, E. J. & SOLIS, S. R. 1988 Measurement of the local wavenumber and frequency spectrum in a plane wake. *Exp. Fluids* **6**, 365–372.

KELLY, R. E. 1967 On the stability of an inviscid shear layer which is periodic in space and time. *J. Fluid Mech.* **27**, 657–689.

KIM, K. I. & POWERS, E. J. 1988 A digital method of modeling quadratically nonlinear systems with a general random input. *IEEE Trans. Acoustics, Speech, Signal Processing* **36**, 1758–1769.

KIM, S. B., POWERS, E. J., MIKSAD, R. W. & FISCHER, F. J. 1991 Quantification of nonlinear energy transfer to sum and difference frequency responses of TLP's. *Proc. First Intl Offshore and Polar Engng Conf. Edinburgh, UK.*

KIM, Y. C. & POWERS, E. J. 1979 Digital bispectral analysis and its applications to nonlinear wave interactions. *IEEE Trans. Plasma Sci.* **PS-7**, 120–131.

MANKBADI, R. R. 1985 The mechanism of mixing enhancement and suppression in a circular jet under excitation conditions. *Phys. Fluids* **28**, 2062–2074.

MIKSAD, R. W. 1972 Experiments on the non-linear stages of free shear layer transition. *J. Fluid Mech.* **56**, 695–719.

MIKSAD, R. W. 1973 Experiments on nonlinear interactions in the transition of a free shear layer. *J. Fluid Mech.* **59**, 1–21.

MONKEWITZ, P. A. 1988 Subharmonic resonance, pairing and shredding in the mixing layer. *J. Fluid Mech.* **188**, 223–252.

MONKEWITZ, P. A. & HUERRE, P. 1982 The influence of the velocity ratio on the spatial instability of mixing layers. *Phys. Fluids* **25**, 1137–1143.

NIKITOPOULOS, D. E. & LIU, J. T. C. 1987 Nonlinear binary-mode interactions in a developing mixing layer. *J. Fluid Mech.* **179**, 345–370.

PATNAIK, P. C., SHERMAN, F. S. & CORCOS, G. M. 1976 A numerical simulation of Kelvin–Helmholtz waves of finite amplitude. *J. Fluid Mech.* **73**, 215–240.

RAETZ, G. S. 1959 A new theory of the cause of transition in fluid flows. *Norair Rep.*, NOR-59-383, Hawthorn, CA.

RAJAEE, M. & KARLSSON, S. K. F. 1992 On the Fourier space decomposition of free shear flow measurements and mode degenerating in the pairing process. *Phys. Fluids* A **4**, 321–339.

RILEY, J. J. & METCALFE, R. W. 1980 Direct numerical simulation of a perturbed mixing layer. *AIAA Paper* 80-0274.

RITZ, CH. P. 1991 Digital spectral analysis of plasma fluctuations. *Lecture Notes of Summer School on Plasma Turbulence and Transport, Madison, Wisconsin.*

RITZ, CH. P. & POWERS, E. J. 1986 Estimation of nonlinear transfer functions for fully developed turbulence. *Physica D* **20D**, 320–334.

RITZ, CH. P. & POWERS, E. J. & BENGTSON, R. D. 1989 Experimental measurement of three-wave coupling and energy cascading. *Phys. Fluids* B **1**, 153–163.

RITZ, CH. P., POWERS, E. J., MIKSAD, R. W. & SOLIS, R. S. 1988 Nonlinear spectral dynamics of a transitioning flow. *Phys. Fluids* **31**, 3577–3588.

YANG, Z. & KARLSSON, S. K. F. 1991 Evolution of coherent structures in a plane shear layer. *Phys. Fluids* A **3**, 2207–2219.

ZHANG, Y. Q., HO, C. M. & MONKEWITZ, P. A. 1983 The mixing layer forced by fundamental and subharmonic. *Proc. Second IUTAM Symp. on Laminar–Turbulent Transition, Novosibirsk, 1984* (ed. F. F. Kozlov). Springer.